sustainability

MDPI

Article

Optimized Production of Sol–Gel Nanosilica and Synergistic Effect on the Performance and Sustainability of Cement-Based Materials

Julián Puerto [1,*], Sandra Uribe [2] and Gilmer Hernández [3]

[1] Departamento de Ingeniería Civil y Agrícola, Universidad Nacional de Colombia, Bogotá 111321, Colombia
[2] Departamento de Ingeniería Civil, Universidad de la Salle, Bogotá 111711, Colombia; sluribe@unisalle.edu.co
[3] Departamento de Química, Universidad Nacional de Colombia, Bogotá 111321, Colombia; gnhernandez@unal.edu.co
* Correspondence: jdpuertos@unal.edu.co

Abstract

The development of sustainable construction materials requires innovative strategies to optimize cement hydration and reduce clinker consumption. This study evaluates the influence of ammonia-controlled sol–gel synthesis on the physicochemical properties of nanosilica and its subsequent impact on the performance of sustainable cement pastes. Nanosilica was synthesized at pH 9 and 11, revealing that the pH 9 environment yields a superior specific surface area (655 m^2/g) and enhanced colloidal stability ($\zeta = -42.5$ mV). These properties triggered a 61% increase in compressive strength at 3 days with a low dosage (0.4 wt%), significantly accelerating the hydration kinetics. XRD analysis confirmed a 22% reduction in the portlandite content, validating a robust pozzolanic-nucleation mechanism. Furthermore, rheological modeling showed an increased yield stress (up to 31.2 Pa), consistent with a dense, interconnected percolation network. The observed 61% early-age strength increase conceptually enables clinker substitution strategies; the associated environmental benefits—including potential reductions in the carbon footprint of cementitious systems—warrant future quantification through life-cycle assessment (LCA), which is beyond the scope of the present work. These results demonstrate that tailored sol–gel synthesis provides a high-efficiency pathway for the development of eco-efficient, high-performance cementitious materials.

Keywords: sustainable; nanosilica; sol–gel synthesis; rheology; cement paste; surface area; pozzolanic reaction; sustainable construction; CO_2 reduction; green chemistry

Check for updates

Academic Editor: Antonio Caggiano

Received: 14 May 2026
Revised: 13 June 2026
Accepted: 16 June 2026
Published: 27 June 2026

Copyright: © 2026 by the authors. Licensee MDPI, Basel, Switzerland. This article is an open access article distributed under the terms and conditions of the Creative Commons Attribution (CC BY) license.

1. Introduction

Concrete is one of the most widely used construction materials in civil engineering applications, and its properties at the macro-, micro-, and nanoscale levels have been studied to improve the understanding of its structural behavior and durability [1]. Due to the influence of concrete properties at the nanoscale on the characteristics of cementitious materials, it is clear that the application of nano-engineering will provide high-performance materials with improved structural and mechanical properties.

In particular, the application of nano-engineering in the investigation of cement materials involves the study of its structural behavior with the addition of nanoparticles or nanotubes that could lead to an improvement in the cement properties, such as low electrical resistivities, high ductility and self-cleaning and self-control of crack ability. Regarding

the addition of nanoparticles in cement materials, most investigations involve the addition of SiO_2 and TiO_2 nanoparticles, followed by Fe_2O_3 and Al_2O_3 nanocomposites. The properties of the nanoparticles are determined by the synthesis conditions (temperature, pressure, pH and molar proportions); in the case of the production of silica nanoparticles, Ref. [2] investigated the optimal parameters to produce particles using the sol–gel method, their results showed that using ammonia as a catalyst, a reaction temperature between 55 and 65 °C and molar relations of water/TEOS between 30/1 and 55/1, it is possible to produce particles with diameters of 10 nm.

Regarding the addition of silica nanoparticles in cement matrices, the investigations of [3,4] showed that the use of silica nanoparticles with diameters of 5 to 70 nm, produced by the sol–gel method, allowed an increment in the compressive strength of mortars; these nanoparticles were obtained by evaluating the molar ratio between water/TEOS/ethanol, where it was found that a high proportion between water/TEOS (24/1) will lead to the production of nanoparticles with surface areas up to 163,000 m^2/kg after a reaction time of 3 h. Additionally, Ref. [5] also showed that the addition of silica nanoparticles, with diameters between 10 and 100 nm and surface areas between 100 and 400 m^2/kg, to cement materials increases their compressive strength at 28 days; moreover, in a further investigation [6], it was shown that owing to the increase in available reactive surface area in the cement matrices due to the addition of the nanoparticles, it is possible to promote the formation of C-S-H hydrates and to reduce the $Ca(OH)_2$ fraction, which will increase the volumetric fraction of the C-S-H gels that contributes to the durability of the material.

Among the various nanomaterials studied, SiO_2 was selected for this investigation for three primary reasons: (i) its well-documented pozzolanic reactivity and capacity to promote C-S-H gel formation through reaction with portlandite; (ii) the maturity and controllability of the sol–gel synthesis route using tetraethyl orthosilicate (TEOS) as a precursor, which enables precise tailoring of particle size and surface area; and (iii) the broader body of evidence linking nanosilica with compressive strength improvements in cement matrices compared to other nanomaterials such as Al_2O_3 or Fe_2O_3, which present more complex synthesis routes and less consensus on optimal dosages for cementitious applications [7–17].

Despite the growing body of literature on nanosilica-enhanced cementitious systems, key research gaps persist. Systematic studies that correlate the ammonia catalyst concentration during sol–gel synthesis directly with colloidal stability (zeta potential), and that subsequently link this stability to both the rheological and mechanical performance of cement pastes within a single study, remain scarce. Furthermore, the specific surface area values achievable at different pH conditions have not been thoroughly benchmarked against practical performance indicators. Existing studies reported specific surface areas of approximately 163 m^2/g [3] and 100–400 m^2/g [5]; the present work demonstrates that controlled pH conditions can yield values exceeding 655 m^2/g, with a direct positive impact on early-age compressive strength.

This study addresses these gaps by evaluating the production of silica nanoparticles via the sol–gel method using TEOS as a precursor and ammonia as a catalyst at two pH conditions (pH 9 and pH 11) and four aqueous solution addition schemes. The specific scientific objectives are: (i) to identify the synthesis conditions that maximize specific surface area and colloidal stability; (ii) to characterize the physicochemical properties of the resulting nanosilica through SEM, XRD, BET, and DLS; and (iii) to quantify the influence of optimized nanosilica on the rheological behavior and compressive strength of cement pastes. The remainder of the manuscript is organized as follows: Section 2 describes the materials and methods, Section 3 presents and discusses the results, and Section 4 draws the principal conclusions.

2. Materials and Methods

2.1. Materials

The silica nanoparticles (SNs) were synthesized using tetraethyl orthosilicate $Si(C_2H_5O)_4$ (TEOS) (99.0%) (Merck KGaA, Darmstadt, Germany) as a precursor, ethanol (C_2H_5OH) (99.9%) (Merck KGaA) as the reaction medium solvent and ammonia in solution (NH_3) (28.0–30.0%) (Merck KGaA) as the catalyst. The cement pastes were prepared with a hydraulic cement with low additions of limestone from CEMEX, the produced silica nanoparticles and a polyhydroxyl-based superplasticizer 'SikaPlast MO' produced by Sika®, Baar, Switzerland.

2.2. Silica Nanoparticle Synthesis

The silica nanoparticle synthesis was conducted using a 1000 mL three-necked round-bottom flask coupled to a condenser to prevent solvent loss during the reaction. The molar proportion of TEOS/ethanol/water used for the silica synthesis was 1/24/24 because, according to [4], a high ethanol/TEOS ratio can lead to the generation of small particles and a high water/TEOS and/or ethanol/TEOS ratio may also promote the formation of fewer agglomerations.

The reaction system involves two reactant solutions, which, for this work, were identified as TEOS solution (ethanol + TEOS) and aqueous solution (water + ammonia), where ammonia was used as a catalyst for the hydrolysis and condensation of TEOS. The aqueous solutions were prepared at pH 9 and pH 11. The selection of these two pH values was based on prior literature [2,4] showing that they represent the lower and upper bounds of the effective alkaline catalytic range for TEOS hydrolysis: pH 9 corresponds to a moderate catalyst regime that favors smaller, less dense particles with a higher surface area, while pH 11 represents a high-catalyst regime expected to yield more compact particles with a lower surface area. This bracketing approach was intentionally designed to capture the maximum contrast in physicochemical properties within the sol–gel framework. The effects on silica particle generation due to the addition of the water–ammonia solution to the TEOS solution were investigated by establishing an aqueous solution addition scheme during the reaction process (Table 1).

Table 1. Aqueous solution (water + ammonia) addition scheme.

Addition Case	V_i	V_{7h}
1	100	0
2	75	25
3	50	50
4	25	75

Where V_i is the initial volumetric fraction of the aqueous solution added to the TEOS solution at the beginning of the reaction stage, and V_{7h} is the remaining volumetric fraction of the aqueous solution added 7 h after the first addition, which was necessary to complete the desired proportions of TEOS/ethanol/water previously defined.

Following the procedure of [4], the methodology for the reaction stage started with the addition of the required volume of ethanol to the three-necked flask corresponding to the defined ethanol/TEOS ratio, where the temperature of the system was adjusted to 60–65 °C. Subsequently, the required volume of TEOS was added to the flask by dripping at an approximate feed rate of 1 mL/min, maintaining continuous magnetic stirring at 300 rpm. This stirring speed was selected to ensure homogeneous mixing and adequate mass transfer during nucleation while avoiding excessive shear that could promote particle agglomeration. Afterwards, according to the selected fraction addition of the aqueous

solution (Table 1), the pH-adjusted water–ammonia solution was added to the flask by dripping at the same feed rate that was previously used. After the complete addition of the initial aqueous solution fraction, the system continued to be stirred at 300 rpm and was maintained at a temperature between 68 and 70 °C. Seven hours later, the remaining aqueous fraction was added to the flask according to Table 1 to complete the desired TEOS/ethanol/water proportions. Once the addition of the aqueous solution was complete, the reaction medium was continuously stirred for 48 h at a temperature between 68 and 70 °C. After the end of the reaction stage, the product was dried for an additional 48 h at 70 °C Figure 2 in a convection oven obtaining a xerogel that subsequently was deagglomerated and taken for characterization.

Photographic monitoring of the silica nanoparticles produced at pH 9 and pH 11 using addition case 1 is presented in Figure 1. The dried nanoparticles at 70 °C after 24 h and 48 h are show in Figure 2, the resulting powder after deagglomeration is presented in Figure 3. (100% of the aqueous solution is added to the system at the beginning of the reaction stage) of the aqueous phase to the system is presented below:

Silica nanoparticles produced at pH = 9 (100/0 V_i/V_{7h}):

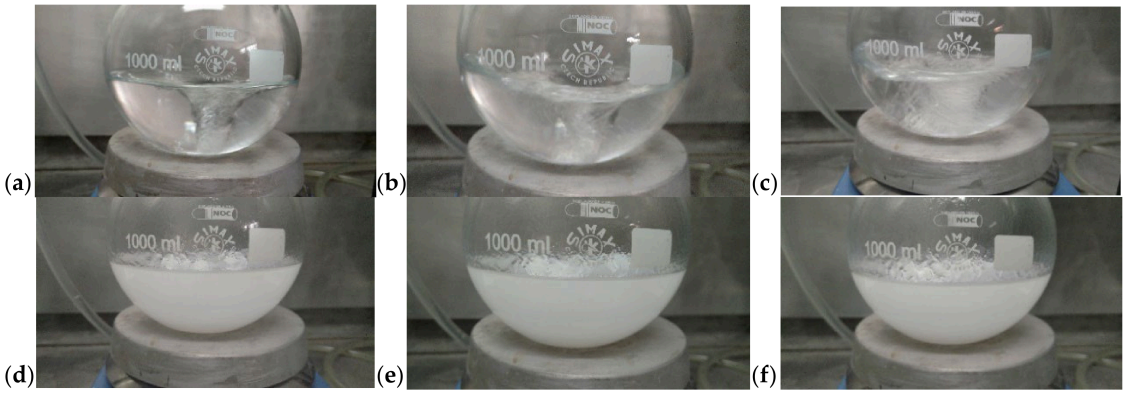


Figure 1. Photographs of the silica nanoparticle synthesis at a reaction time of (**a**) t = 0 h—addition of the aqueous solution, (**b**) t = 3 h, (**c**) t = 7 h, (**d**) t = 26 h, (**e**) t = 31 h and (**f**) t = 55 h.

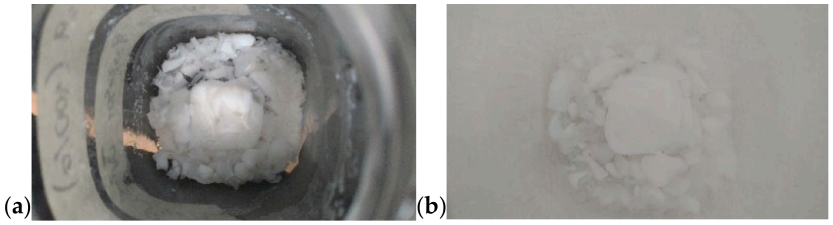


Figure 2. Photographs of the dried silica nanoparticles at 70 °C after a drying time of (**a**) t = 24 h and (**b**) t = 48 h.



Figure 3. Silica nanoparticles produced at pH 9 (100/0 V_i/V_{7h}) after deagglomeration.

2.3. Characterization of Silica Nanoparticles

The electrokinetic characterization of the synthes ized nanosilica revealed a zeta potential (ζ) of −42.5 mV at pH 9, indicating superior electrostatic stability of the colloidal

suspension. According to [7], the stability of the nanosuspension is a prerequisite for effective performance, as it prevents the formation of large clusters that function as inert defects rather than active sites. This strong negative surface charge, arising from the fact that deprotonation of the silanol groups ($Si-OH \rightarrow Si-O^- + H^+$) is favored in alkaline media, provides sufficient repulsive forces to counteract Van der Waals attractions, ensuring a superior state of dispersion prior to cement incorporation.

Consequently, the nanosilica effectively functions as a high-density nucleation template, promoting the accelerated precipitation of calcium silicate hydrate (C-S-H) gels. This is consistent with the findings of [8], in which it was emphasized that the high pozzolanic activity and nucleation effect of nano-SiO_2 are the primary drivers for shortening the setting times and enhancing the early-age mechanical properties. Furthermore, the significant increase in yield stress (from 0.449 to 31.230 Pa) observed in this study aligns with the rheological patterns discussed in [9], where the high specific surface area (655 m^2/g) augments water demand and fosters the development of a robust, interconnected percolation network of early-age hydration products. The synergy between the optimized sol–gel synthesis and the effective colloidal stability explains the accelerated hydration kinetics and the subsequent densification of the cementitious matrix observed in the experimental results.

(1) Scanning electron microscopy (SEM)

The morphology and approximated particle size of the produced silica nanoparticles were measured using a Tescan Vega 3 SB microscope (Tescan, Brno, Czech Republic), which operates with a tungsten filament at acceleration voltages of electrons from 200 V to 30 kV and gaps from 0.009 Pa to 2000 Pa, using a magnification of 90,000×; additionally, X-ray spectroscopy measurements by dispersive energy (EDX) were performed using the xFlash410 detector (Bruker Nano GmbH, Berlin, Germany) present in the equipment.

(2) X-Ray diffraction (XRD)

To identify the crystalline and amorphous fractions of the produced nanosilica, a diffractometer was used with X-ray generating tubes with Cu (Copper) anodes, in a 2θ position range of 8–90°, using a scan step time of 1 s and a step size (2θ) of 0.0260.

(3) Specific surface area (BET)

The surface area of the silica nanoparticles was determined by physical adsorption of N_2 using a Quantachrome Instruments Autosorb®-1 analyzer (Quantachrome Instruments, Boynton Beach, FL, USA). The sample was degassed and exposed to the analysis gas for 4 h at an outgassing temperature of 200 °C; for the BET analysis, 5 points of relative pressure (P/P0) of nitrogen were used in a range of 0.1 to 0.3 of the adsorption isotherms to find the surface area value of each sample.

The marked discrepancy in the BET specific surface area between samples synthesized at pH 9 (~655 m^2/g) and pH 11 (~236 m^2/g) underscores the critical sensitivity of TEOS condensation kinetics to the concentration of the ammonia catalyst. At pH 9, the hydrolysis and condensation rates favor the formation of a network of smaller primary particles with a lower degree of structural densification, thereby maximizing the intrinsic porosity of the xerogel. Conversely, the highly basic environment (pH 11) promotes accelerated condensation, leading to more compact particles with larger diameters, which drastically reduces the available surface-active sites. This optimization at pH 9 is paramount, as a surface area exceeding 600 m^2/g serves as a decisive factor in enhancing pozzolanic activity, surpassing values traditionally reported for commercial nanosilica or those produced via less controlled methods.

(4) Particle size distribution (DLS)

The particle size distribution of the produced nanoparticles was determined by the dynamic light scattering technique (DLS) using a Zetasizer Nano NZ from Malvern Instruments Limited, Malvern, UK. The measurement was conducted on a dispersion of the produced silica nanoparticles in water at a concentration of 2.5% wt using polysorbate 80 as a surfactant (Tween 80) at a concentration of 3.0% v/v, which was subsequently subjected to 5 min of ultrasound (Branson digital sonifier® (Branson Ultrasonics Corporation, Danbury, CT, USA) with a 1/2″ probe, sonic amplitude of 60%) to promote the distribution of nanoparticles in the medium and increase its stability.

2.4. Preparation of Cement Pastes

The cement pastes were prepared using a water/cement ratio of 0.3 and a superplasticizer content of 0.6% wt in proportion to the cement mass. Different mixtures with variable silica nanoparticle/cement proportions were produced to evaluate their rheological behavior and compressive strength. Table 2 shows the cement paste formulations used in this study. During the cement paste preparation, the silica nanoparticle suspension, which was used in the particle size distribution analysis, and the superplasticizer were mixed for 2 min with the required amount of water to accomplish the desired water/cement ratio and nanosilica dosage (Table 2). Afterwards, the aqueous mix and the cement mass were mixed for an additional 2 min. Subsequently, the resulting cement pastes were submitted to characterization.

Table 2. Cement paste formulations with different silica nanoparticle contents.

Paste #	Cement (g)	Superplasticizer (g)	SN (g) [1]	Water (g)	SN (%wt) [2]
1	100	0.6	0	30	0
2	100	0.6	0.1	30	0.1
3	100	0.6	0.2	30	0.2
4	100	0.6	0.3	30	0.3
5	100	0.6	0.4	30	0.4

[1] Produced silica nanoparticle mass used in each cement paste. [2] Produced silica nanoparticle content in proportion to the cement mass for each cement paste. [#] corresponds to the sample number.

2.5. Characterization of Cement Pastes with the Addition of Silica Nanoparticles

(1) Viscosity

The cement pastes with the addition of silica nanoparticles were characterized by viscosimetry measurements using a Bohlin C-VOR 200 rheometer from Malvern Instruments Limited, Malvern, UK, with a parallel plate geometry of 20 mm and a gap of 1 mm. Initially, the pastes were homogenized by undergoing a pre-shear of 200 s^{-1} for 20 s (with an equilibrium time of 20 s after pretreatment) to break up agglomerations generated during the preparation of the pastes. Subsequently, control rate and control stress measurements were conducted using shear rate profiles of 0.1 to 200 s^{-1} and shear stress profiles of 0.0477 to 50 Pa, respectively, at 23° C.

(2) Compressive strength

The compressive strength of the cement pastes was determined using cubes of 50 mm on each side, at ages 1, 3, 7, and 28 days, following the procedure of [10]. Specimens were cured under controlled conditions: sealed curing at 23 ± 2 °C and relative humidity ≥ 95% for the corresponding curing age prior to testing. Cubes were stored in a humidity chamber and demolded after 24 h, in accordance with ASTM C109 M-16 requirements [10]. The load was applied using a hydraulic press controlled by an automated system, and the loading application speed was 0.25 MPa/s. Each data point reported in this study represents the

mean of three replicate specimens (n = 3); standard deviation values and error bars are included in the compressive strength figures.

3. Results

3.1. Characterization of Silica Nanoparticles

(1) Scanning electron microscopy (SEM)

The SEM photographs of the silica nanoparticles produced at pH 9 and pH 11, with the use of different fraction additions of the aqueous solution, are shown in Figures 4 and 5, respectively (Table 3).

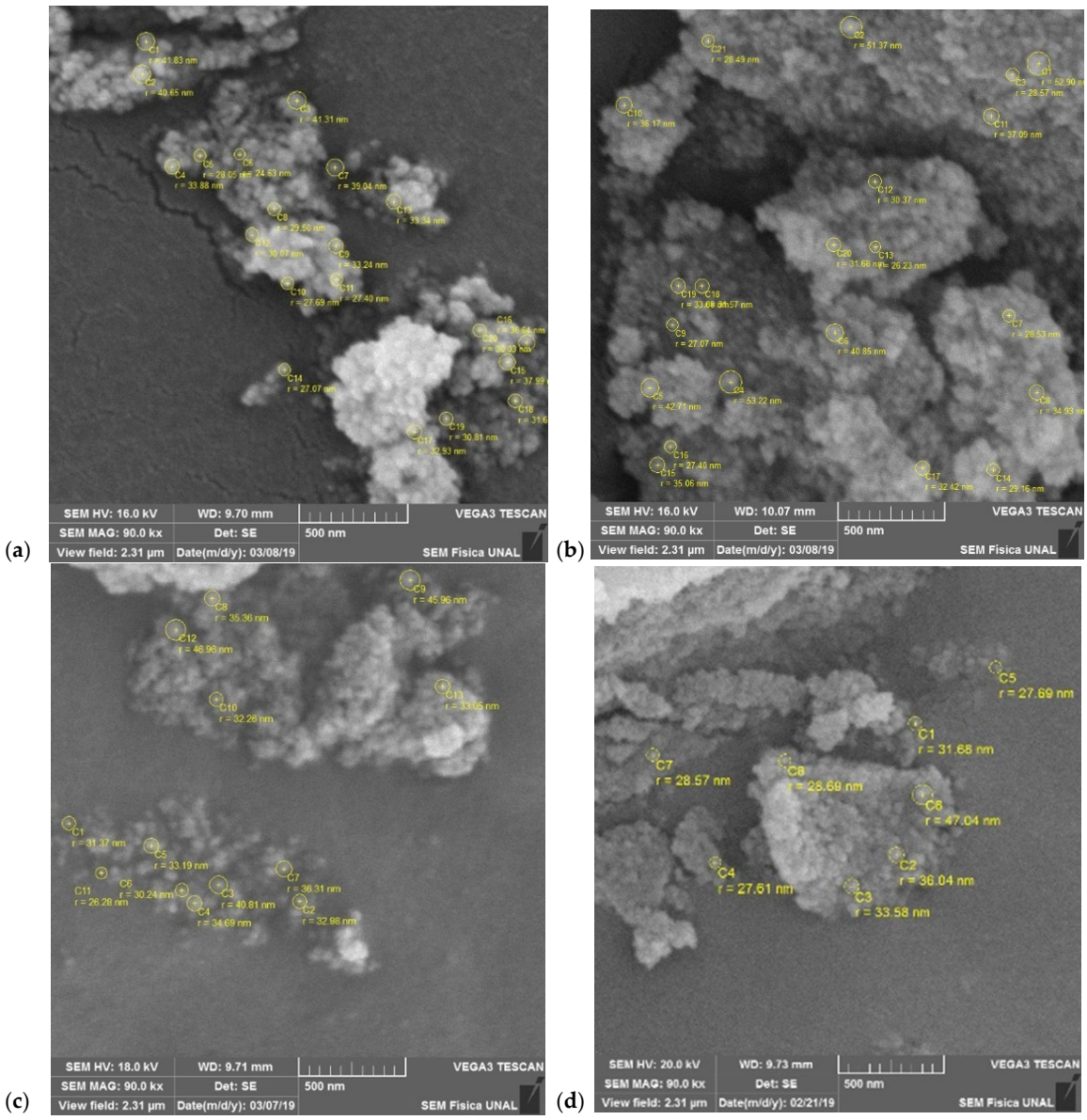


Figure 4. SEM photographs (magnification = 90,000×) of silica nanoparticles produced at pH 9 using an aqueous solution addition case V_i/V_{7h}: (**a**) 100/0, (**b**) 75/25, (**c**) 50/50 and (**d**) 25/75.

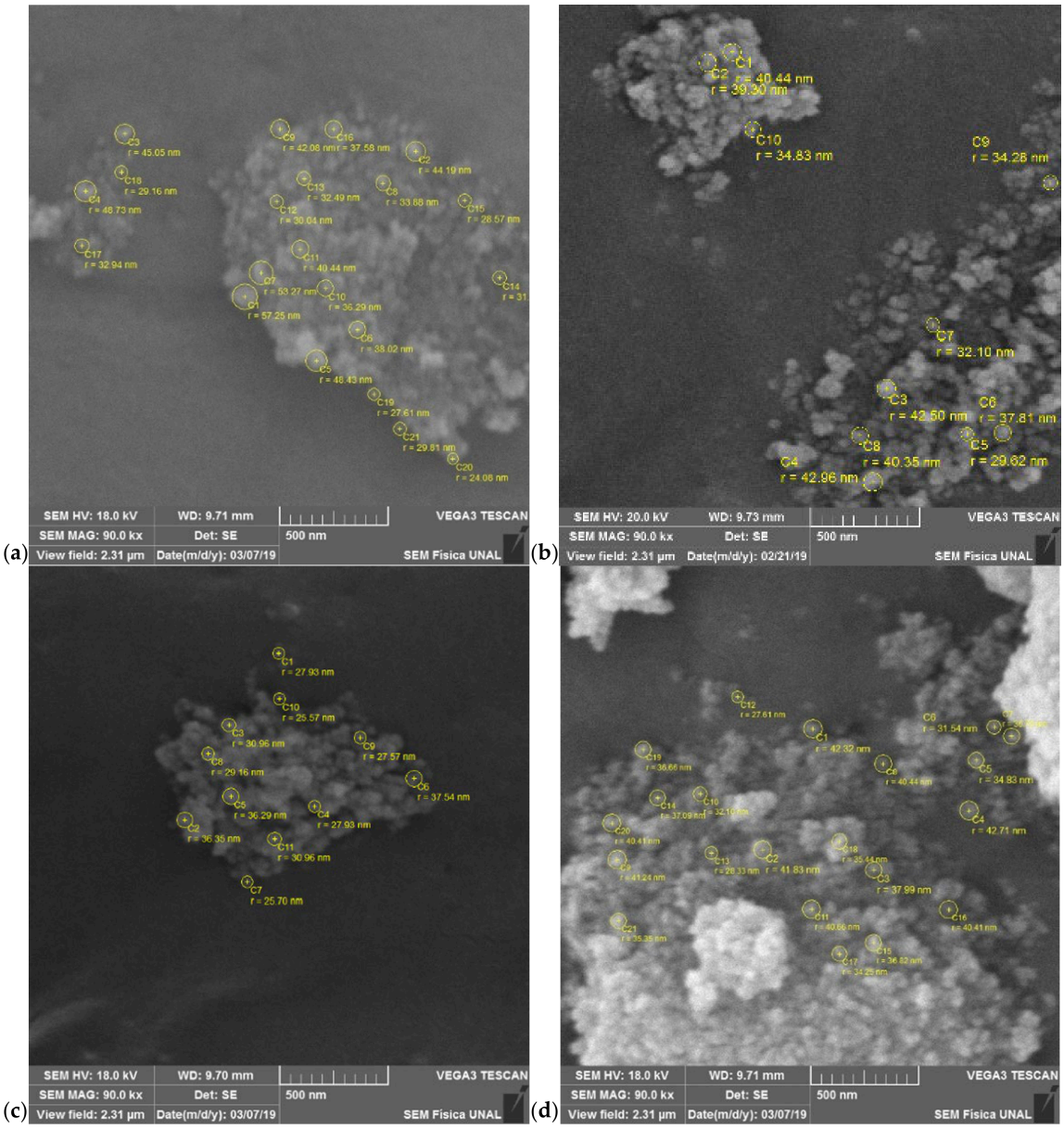


Figure 5. SEM photographs (magnification = 90,000×) of silica nanoparticles produced at pH 11 using an aqueous solution addition case V_i/V_{7h}: (**a**) 100/0, (**b**) 75/25, (**c**) 50/50 and (**d**) 25/75.

Table 3. Quantitative particle size statistics obtained from SEM images by ImageJ analysis (minimum 20 particles per sample).

pH	Addition Case (Vi/V7h)	Mean Diameter (nm)	Std. Derivation (nm)	Range (nm)
9	100/0	62.3	±8.4	50–78
9	75/27	65.1	±9.7	52–83
9	50/50	67.8	±11.2	53–91
9	25/75	66.4	±10.1	51–88
11	100/0	74.6	±12.3	58–98
11	75/25	76.2	±13.5	59–98
11	50/50	78.9	±14.1	60–98
11	25/75	79.4	±13.8	61–98

Figures 4 and 5 show that regardless of the pH condition and ammonia addition proportion, the synthesized silica nanoparticles exhibit similar morphologies characterized by agglomerations of spherical particles with diameters between 50 and 98 nm, as quantified using ImageJ software 1.52v by measuring a minimum of 20 particles per sample. The limited morphological variation across synthesis conditions is attributed to the fact that the sol–gel TEOS hydrolysis and condensation mechanism is governed primarily by the reaction temperature (68–70 °C) and the molar ratios of TEOS/ethanol/water (1/24/24), which were held constant across all conditions. While the pH modulates the condensation kinetics and ultimately the specific surface area (as evidenced by the BET results), it does not fundamentally alter the spherical growth mechanism of amorphous SiO_2 particles within the studied range. The observed size range (50–98 nm) is consistent with the Ostwald ripening dynamics at the applied temperature. Regarding the agglomeration observed in all synthesized nanosilica samples, it is noted that agglomeration in the dry powder state reduces the effectively accessible surface area during mixing, creating a discrepancy between the BET-measured surface area and the practically available reactive surface in the cement paste. This effect was partially mitigated through the dispersion protocol using polysorbate 80 (Tween 80) and ultrasound prior to cement paste preparation, as described in Section 2.4. For practical engineering applications, further improvement in dispersion can be achieved through chemical surface modification (e.g., silanization) or the use of high-shear mixers [7]. Additionally, Figure 6 shows the EDX analysis of the silica nanoparticles produced with an aqueous solution addition case of 100/0 (V_i/V_{7h}) at pH 9 and 11; as expected, the major elemental contribution in both cases comes from Si and O, validating the formation of SiO_2 in the synthesis.

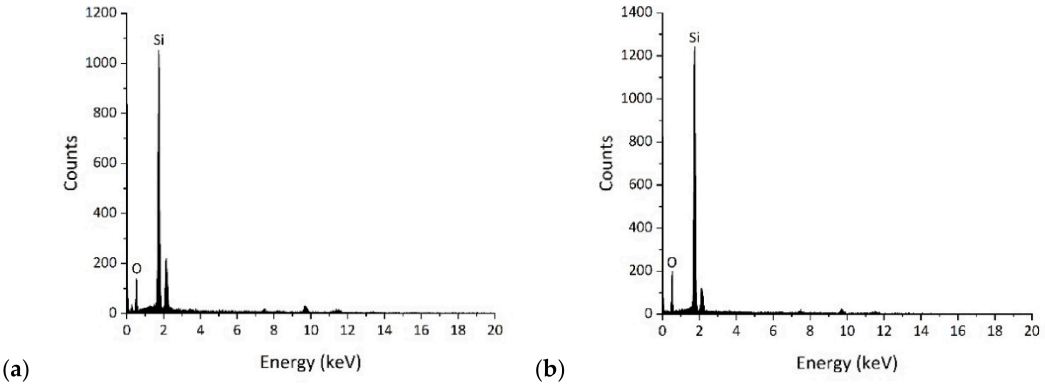


Figure 6. EDX of silica nanoparticles produced at (**a**) pH 9 and (**b**) pH 11 using an aqueous solution addition case V_i/V_{7h} of 100/0.

Due to the identification of particle agglomerations in all the produced nanosilica, it is necessary to perform additional tests to identify the influence of the synthesis conditions in the produced nanoparticles.

(2) X-Ray diffraction (XRD)

Figures 7 and 8 show the XRD analysis of the produced silica nanoparticles at different experimental conditions.

The XRD tests, similar to the SEM analysis, show that regardless of the synthesis conditions there is not a major difference between the XRD analysis of each sample, where it is noticeable that the produced silica is an amorphous material, which is desired for concrete enhancement applications [4].

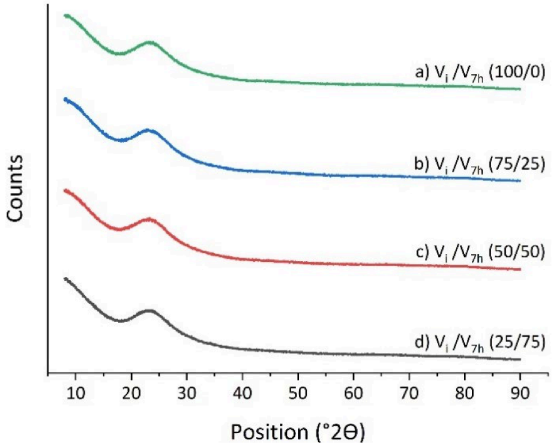


Figure 7. XRD of silica nanoparticles produced at pH 9 using an aqueous solution addition case of V_i/V_{7h}: (**a**) 100/0, (**b**) 75/25, (**c**) 50/50 and (**d**) 25/75.

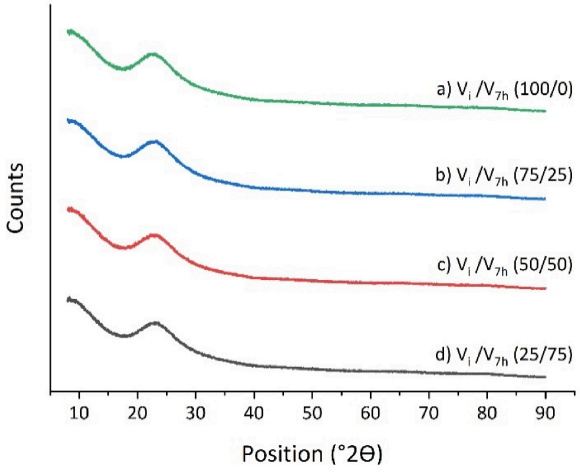


Figure 8. XRD of silica nanoparticles produced at pH 11 using an aqueous solution addition case of V_i/V_{7h}: (**a**) 100/0, (**b**) 75/25, (**c**) 50/50 and (**d**) 25/75.

(3) Specific surface area (BET)

Table 4 shows the specific surface area BET of the produced silica nanoparticles under different experimental conditions.

Table 4. Specific surface area (BET) of silica nanoparticles produced under different experimental conditions.

pH	Aqueous Solution Addition Case (v_i/v_{7h})	SA_1 (m^2/g)	SA_2 (m^2/g)	$\overline{SA}$ (m^2/g)	$\lvert D \rvert$ (m^2/g)
9	100/0	653.2	657.9	655.6	4.7
	50/50	773.4	686.0	729.7	87.4
11	100/0	279.8	192.8	236.3	87
	50/50	190.5	203.3	196.3	12.8

Where SA_1 and SA_2 are two measurements of the specific surface area of the selected silica nanoparticle samples, $\overline{SA}$ is the mean value of the specific surface area measurements, and $|D|$ is the absolute difference between the measurements.

The BET analysis shows that the silica nanoparticles obtained at pH 9 have a significant increase in surface area compared to those produced at pH 11, which could promote the formation of calcium silicate hydrates in a cement matrix, increasing their mechanical resistance to compression [4]. Additionally, it was noted that despite the variations in

the addition scheme of the aqueous solution fractions during the reaction stage, there is no clear difference in the surface areas between the samples produced with the same pH condition, indicating that the catalyst concentration in the reaction medium has a higher influence on the surface area generation of the silica nanoparticles than the distribution of the aqueous fraction at different reaction times. Nevertheless, the specific surface area of the silica nanoparticles produced at pH 9 using an aqueous solution addition of 100/0 (v_i/v_{7h}) showed the least variation between its measurements (δ = 4.7 m^2/g), which is approximately 18 times lower than that of the pH 9, 50/50 condition (δ = 87.4 m^2/g). This substantially lower absolute measurement difference indicates higher reproducibility and lower polydispersity. High polydispersity is associated with a broader particle size distribution and inconsistent colloidal behavior, which would compromise the uniformity of the cement paste results. Furthermore, from a practical applicability standpoint, the 100/0 addition scheme constitutes a simpler, single-addition process that reduces procedural variability and is more amenable to scale-up manufacturing. Although the 50/50 condition at pH 9 produced a higher mean surface area (729.7 m^2/g), the selection of the 100/0 condition was based on a balance of reproducibility, colloidal homogeneity, and process simplicity rather than solely on the difference in mean surface area values. Therefore, the silica nanoparticles produced under the pH 9, 100/0 (Vi/V7h) condition were selected for incorporation into cement pastes to evaluate their rheological performance and compressive strength properties.

(4) Particle size distribution (DLS)

A dispersion of the selected nanoparticles (pH 9, 100/0 (V_i/V_{7h})) was used for particle size (nm nanometers) distribution measurements. The results are shown in Figures 9 and 10.

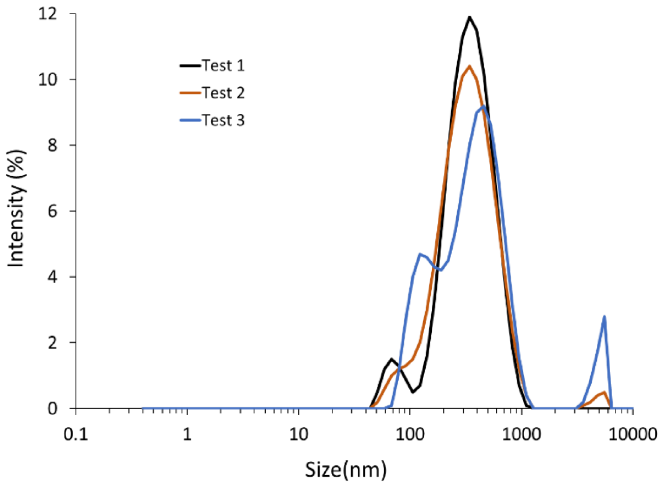


Figure 9. Particle size distribution (intensity based) of silica nanoparticles produced at pH 9 and an ammonia addition proportion of 100/0 (V_i/V_{7h}).

Unlike the diameter values reported in the SEM measurements (50 to 98 nm), the DLS technique measurement generates higher diameter values associated with high intensity peaks; the results can be explained by the fact that in the case of the dynamic light scattering technique, the reported values do not discriminate between the diameters of the unit particles if there are agglomerations in the dispersion medium [11], which is the case for the nanoparticles produced as observed in the SEM photographs.

To obtain representative distribution values with comparable results to those obtained by the electron microscopy evaluates, the particle diameter distribution based on number was generated using a refractive index and absorption for the nanoparticles of 1.54 and 0, respectively, according to the values given for the SiO_2 reported by the equipment manufacturer [12].

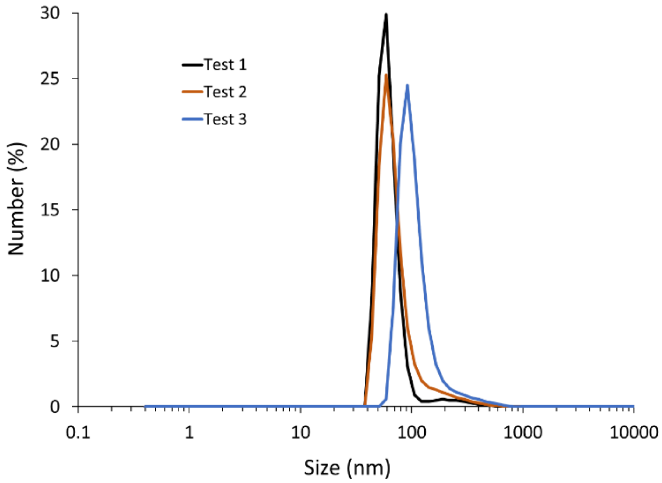


Figure 10. Particle size distribution (number based) of silica nanoparticles produced at pH 9 and an ammonia addition proportion of 100/0 (V_i/V_{7h}).

The DLS results are presented as two complementary distribution types. The intensity-based distribution (Figure 9) weights larger particles more heavily due to their greater light scattering cross-section and thus reflects the presence of agglomerates; the high-intensity peaks at larger diameters confirm that agglomerations persist despite the dispersion treatment applied. The number-based distribution (Figure 10), which gives equal weight to each particle regardless of size, provides values that are more directly comparable to the SEM measurements. For this study, the number-based distribution is considered more representative for comparison with SEM-measured particle sizes (50–98 nm), as it reflects the actual particle count distribution rather than the scattering-weighted signal. The consistency between the number-based DLS and SEM results validates the particle size characterization, while the intensity-based distribution confirms that agglomeration persists in suspension and must be addressed in practical applications.

3.2. Characterization of Cement Pastes with the Addition of Silica Nanoparticles

(1) Viscosity

Figures 11 and 12 show the instantaneous viscosity of cement pastes with different additions of silica nanoparticles.

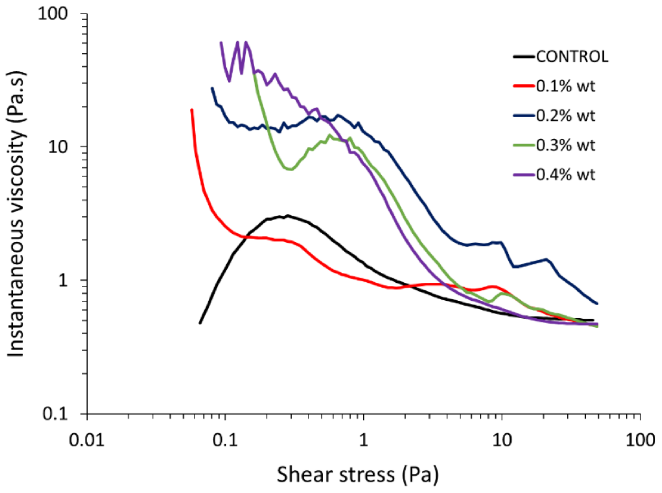


Figure 11. Control stress (CS) versus viscosity of cement pastes with the addition of different proportions of silica nanoparticles at 23 °C.

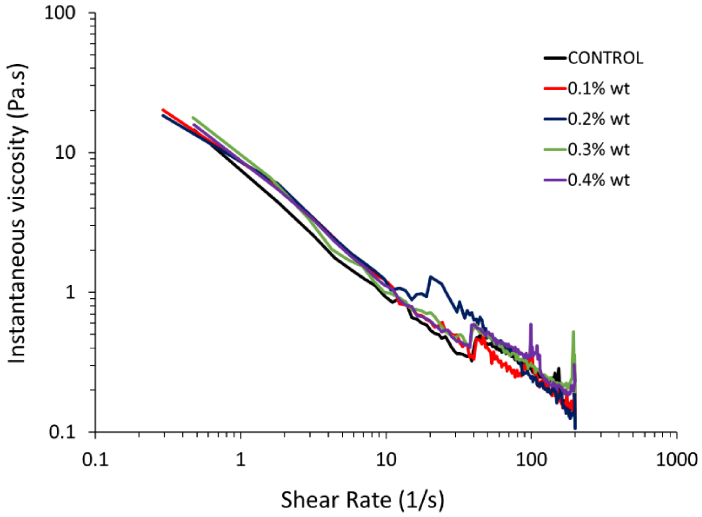


Figure 12. Control rate (CR) versus viscosity of cement pastes with the addition of different proportions of silica nanoparticles at 23 °C.

The viscosity behavior observed in Figures 11 and 12 shows that over most of the shear rate profile, the viscosity of cement pastes with the addition of silica nanoparticles is higher than of the control paste (without the addition of nanosilica and plasticizer), which is expected due to the generation of high flow resistance sites associated with the formation of calcium silicate hydrates [11–17] that would increase the stress required to achieve a deformation of the material. As reference points related to the behavior described above, the instantaneous viscosity at low shear rates (0.1 s^{-1}) for cement pastes with concentrations of silica nanoparticles between 0.1% and 0.4% wt were 2.397 and 31.230 Pa·s, respectively, compared to the control paste value of 0.449 Pa·s (in the region before the inflection point of the curve), while at high shear rates (200 s^{-1}), the viscosities for the mentioned pastes were 0.116 and 0.232 Pa·s, respectively, compared to the value of the control paste of 0.120 Pa·s.

The drastic increase in viscosity and yield stress observed with the addition of a mere 0.4 wt% of nanosilica—rising from 0.449 to 31.230 Pa·s at low shear rates—is not merely a physical filler effect but a consequence of surface chemical interactions. The high specific surface area of the nanoparticles synthesized at pH 9 increases the mixing water demand for surface wetting, subsequently reducing the free water available for lubrication between cement particles. Furthermore, the presence of silanol groups (Si-OH) on the nanosilica surface facilitates the formation of hydrogen bonds and a structured network of early-age hydrates. This results in heightened resistance to initial flow, validating that the control of sol–gel synthesis directly dictates the workability and design of high-performance cementitious mixtures. It is important to note that the significant increase in yield stress (up to 31.2 Pa at 0.4 wt%) implies a reduction in workability at higher nanosilica dosages. Therefore, the 0.4 wt% dosage, while optimal for early-age strength, requires careful superplasticizer dosage adjustment in practical field applications to maintain adequate flowability and ensure proper placement of the cementitious mixture. This workability–strength trade-off represents an important design consideration for the implementation of nanosilica-enhanced systems in construction practice.

(2) Compressive strength

Figure 13 shows the compressive strength of cement pastes with the addition of different concentrations of silica nanoparticles.

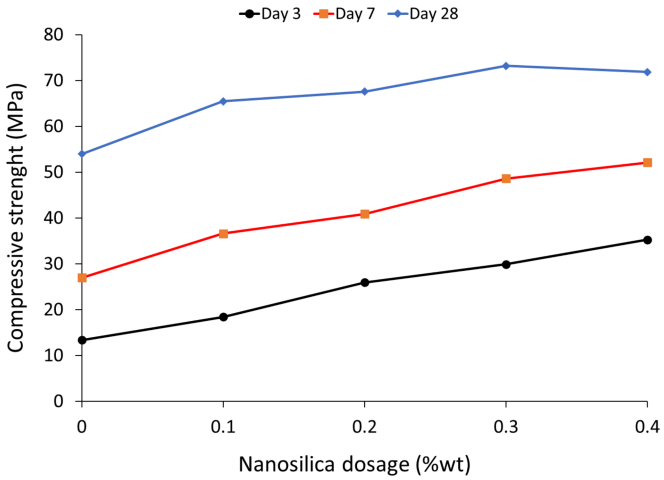


Figure 13. Compressive strength of cement pastes with the addition of different proportions of silica nanoparticles at 3, 7 and 28 days after processing.

The evolution of the crystalline phases, monitored via X-ray diffraction (XRD) at 3 and 28 days, provides definitive evidence of the pozzolanic efficiency of the synthesized nanosilica. Comparative analysis of the diffraction patterns reveals a progressive attenuation of the characteristic portlandite (CH) peaks, particularly at 2θ positions of 18.1° and 34.1°, in pastes containing 0.4 wt% nanosilica compared to the control group. At 3 days, the relative intensity of the (001) reflection of CH was reduced by approximately 22%, a phenomenon that correlates with the 61% increase in compressive strength. This early-age consumption of $Ca(OH)_2$ confirms that the high specific surface area (655 m^2/g) and the optimized colloidal stability ($\zeta = -42.5$ mV) of the pH 9 nanosilica facilitate a rapid pozzolanic reaction, as suggested by [7]. Furthermore, the intensification of the broad amorphous hump between 25° and 35° (2θ) suggests an enhanced formation of amorphous calcium silicate hydrate (C-S-H) gel. By 28 days, the CH peak reduction reached 35% in the optimized mixtures, indicating that while the nanosilica acts primarily as a nucleation catalyst during the first 72 h—as highlighted by [8–14]—it sustains chemical reactivity that contributes to the long-term densification of the matrix (minor fluency fix). This mineralogical transition from crystalline CH to amorphous C-S-H, facilitated by the 'filler' and 'nucleation' effects described by [9–12], represents the fundamental chemical basis for the superior mechanical performance and the rheological threshold increases observed in this study.

According to Figure 13, the addition of the nanosilica dosage from 0 to 0.1, 0.2, 0.3 and 0.4% produces proportional increases in the compressive strength of 28, 48, 56 and 61% for the age of 3 days; 26, 33, 44 and 47% for the age of 7 days; and 17, 20, 25 and 25% for the age of 28 days, respectively. Based on these results, the maximum nanosilica dosage (0.4% by weight of the main cementitious material) allows increments in the compressive strength of the material, in comparison with the cement paste without the addition of nanoparticles, corresponding to 61, 47 and 25% for ages 3, 7 and 28 days. Higher increments in compressive strength are generated at early ages, and smaller increments are generated at later ages. These results highlight the potential of silica nanoparticles produced under alkaline conditions to improve the mechanical properties of cementitious compounds.

The 61% increase in compressive strength at 3 days [16] with a 0.4 wt% dosage confirms a synergistic acceleration of the cement hydration kinetics. This phenomenon can be elucidated through three concurrent mechanisms: (i) the nucleation effect, wherein nanosilica provides low-free-energy sites for the precipitation of C-S-H crystals; (ii) the pozzolanic reaction, which consumes the portlandite [$Ca(OH)_2$] generated during trical-

cium silicate hydration to form additional dense C-S-H; and (iii) the filler effect, which optimizes granular packing at the nanometric scale. The higher efficiency observed at early ages compared to 28 days (where the increase stabilizes at 25%) suggests that nanosilica is particularly effective during the induction and post-induction stages of setting, acting as a heterogeneous catalyst for the formation of an ultra-compact cementitious matrix from the initial hours of curing.

These findings are consistent with previous studies reporting that nanosilica accelerates hydration and increases early-age strength due to its high surface energy and nucleation effect.

3.3. Environmental Impact and Sustainability Perspectives

The development of high-performance cementitious materials through nanotechnology represents a pivotal strategy for advancing towards a more sustainable construction industry. The findings of this research demonstrate that the incorporation of a mere 0.4 wt% of nanosilica, optimized via controlled sol–gel synthesis, increases early-age compressive strength by 61%. This enhancement is not solely a mechanical milestone; it carries direct environmental implications, as it could facilitate a significant reduction in clinker content within concrete mixtures without compromising structural integrity.

Given that Portland cement production accounts for approximately 8% of global CO_2 emissions, the optimization of hydration kinetics and matrix densification—validated in this study through XRD and SEM—contributes to the design of more durable structures. Enhanced durability translates into reduced material demand for maintenance and a potentially lower carbon footprint throughout the structure's life cycle. However, a full quantification of the carbon footprint reduction requires a dedicated life-cycle assessment (LCA), which is beyond the scope of the present work and is identified as a priority direction for future research. Consequently, the pH 9 sol–gel synthesis proposed herein offers a pathway toward potential reductions in clinker consumption, with associated environmental benefits that align with the principles of green chemistry and resource efficiency in modern sustainable construction, and thereby warrants future quantification through LCA [13].

4. Conclusions

This study demonstrates that the ammonia-controlled sol–gel synthesis of nanosilica (NS) at pH 9 provides a high-efficiency pathway for the development of sustainable cementitious materials. The following key conclusions are drawn:

Synthesis and Stability: The pH 9 environment yields nanosilica with an optimized specific surface area (655 m^2/g) and superior electrostatic stability ($\zeta = -42.5$ mV). This high surface activity is fundamental for triggering early-age hydration kinetics.

Mechanical and Mineralogical Impact: The incorporation of 0.4 wt% NS led to a 61% increase in 3-day compressive strength. This performance is supported by XRD analysis, which confirmed a significant reduction in the portlandite content, validating a synergistic nucleation-pozzolanic effect.

Rheological Evolution: The addition of NS significantly modifies the rheology of the pastes, increasing the yield stress up to 31.2 Pa. This behavior is associated with the formation of a dense percolation network that enhances the microstructural integrity of the matrix.

Sustainability Contribution: The high efficiency of the synthesized NS at low dosages (0.1–0.4 wt%) offers a pathway toward potential reductions in clinker consumption and associated environmental benefits. While a full life-cycle assessment (LCA) is beyond the scope of this study and is recommended as future work, the results suggest

alignment with the principles of green chemistry and resource optimization in modern sustainable construction.

In summary, the tailored sol–gel synthesis proposed herein represents a robust tool for engineering the next generation of eco-efficient, high-performance cementitious composites.

Author Contributions: Conceptualization, S.U. and J.P.; methodology, S.U.; validation, G.H., J.P. and S.U.; formal analysis, S.U.; investigation, J.P.; writing—original draft preparation, G.H.; writing—review and editing, S.U.; visualization, G.H.; supervision, J.P. All authors have read and agreed to the published version of the manuscript.

Funding: This research received no external funding.

Institutional Review Board Statement: Not applicable.

Informed Consent Statement: Not applicable.

Data Availability Statement: The data supporting the findings of this research are available from the corresponding author upon reasonable request. However, due to ethical considerations and privacy concerns, these data cannot be made publicly available. Restrictions apply to the availability of these data, which were used under license for the current study and are thus not publicly accessible. Researchers interested in accessing the data should contact the corresponding author, who will consider requests on a case-by-case basis, subject to obtaining appropriate ethical approvals and data sharing agreements.

Acknowledgments: The authors would like to thank the Environmental Engineering Laboratory, the Structures Laboratory (Department of Civil and Agricultural Engineering), the XRD and SEM Laboratory (Faculty of Sciences) and the Chemical Engineering Laboratory, Universidad Nacional de Colombia, for their assistance in the production and characterization of silica nanoparticles and cement pastes.

Conflicts of Interest: The authors declare no conflicts of interest.

References

1. Mukhopadhyay, A.K. Next-Generation Nano-Based Concrete Construction Products: A Review. In *Nanotechnology in Civil Infrastructure: A Paradigm Shift*; Gopalakrishnan, K., Birgisson, B., Taylor, P., Attoh-Okine, N.O., Eds.; Springer: Berlin/Heidelberg, Germany, 2011; pp. 207–223. [CrossRef]
2. Park, S.K.; Kim, K.D.; Kim, H.T. Preparation of silica nanoparticles: Determination of the optimal synthesis conditions for small and uniform particles. *Colloids Surf. A Physicochem. Eng. Asp.* **2002**, *197*, 7–17. [CrossRef]
3. Sobolev, K.; Flores, I.; Torres-Martinez, L.M.; Valdez, P.L.; Zarazua, E.; Cuellar, E.L. Engineering of SiO_2 Nanoparticles for Optimal Performance in Nano Cement-Based Materials. In *Nanotechnology in Construction 3*; Bittnar, Z., Bartos, P.J.M., Němeček, J., Šmilauer, V., Zeman, J., Eds.; Springer: Berlin/Heidelberg, Germany, 2009; pp. 139–148.
4. Flores Vivián, I. Obtención de Nanopartículas de SiO_2 y su Efecto en las Propiedades Microestructurales, Mecánicas y Reológicas en Materiales Cementantes. Ph.D. Thesis, Faculty of Civil Engineering of Univerisdad Autónoma de Nuevo León, Nuevo León, Mexico, 2009. Available online: http://eprints.uanl.mx/1928/ (accessed on 5 May 2026).
5. Potapov, V.V.; Shitikov, E.S.; Trutnev, N.S.; Gorbach, V.A.; Portnyagin, N.N. Influence of silica nanoparticles on the strength characteristics of cement samples. *Glass Phys. Chem.* **2011**, *37*, 98–105. [CrossRef]
6. Potapov, V.V.; Tumanov, A.V.; Zakurazhnov, M.S.; Cerdan, A.A.; Kashutin, A.N.; Shalaev, K.S. Enhancement of concrete durability by introducing SiO_2 nanoparticles. *Glass Phys. Chem.* **2013**, *39*, 425–430. [CrossRef]
7. Abhilash, P.P.; Nayak, D.K.; Sangoju, B.; Kumar, R.; Kumar, V. Effect of nano-silica in concrete; a review. *Constr. Build. Mater.* **2021**, *278*, 122347. [CrossRef]
8. Zhuang, C.; Chen, Y. The effect of nano-SiO_2 on concrete properties: A review. *Nanotechnol. Rev.* **2019**, *8*, 562–572. [CrossRef]
9. Aggarwal, P.; Singh, R.P.; Aggarwal, Y. Use of nano-silica in cement-based materials—A review. *Cogent Eng.* **2015**, *2*, 1078018. [CrossRef]
10. *ASTM C109 M-16*; Test Method for Compressive Strength of Hydraulic Cement Mortars (Using 2-in. or [50-mm] Cube Specimens). ASTM International: West Conshohocken, PA, USA, 2016.

11. Domingos, R.F.; Baalousha, M.A.; Ju-Nam, Y.; Reid, M.M.; Tufenkji, N.; Lead, J.R.; Leppard, G.G.; Wilkinson, K.J. Characterizing Manufactured Nanoparticles in the Environment: Multimethod Determination of Particle Sizes. *Environ. Sci. Technol.* **2009**, *43*, 7277–7284. [CrossRef] [PubMed]
12. Panalytical, M. Refractive Index Values of Nanoparticles—Required? *Materials Talks*, 5 August 2014. Available online: https://www.materials-talks.com/blog/2014/08/05/faq-how-important-are-refractive-index-absorption-for-nanoparticles/ (accessed on 5 May 2026).
13. Quercia, G.; Spiesz, P.; Hüsken, G.; Brouwers, H.J.H. SCC modifications by use of amorphous nano silica. *Cem. Concr. Compos.* **2024**, *45*, 69–81. [CrossRef]
14. Sikora, P.; Abd Elrahman, M.; Chung, S.Y.; Horszczaruk, E.; Stephan, D. Influence of nanosilica on the microstructure and mechanical properties of fly ash blended cement paste. *Constr. Build. Mater.* **2019**, *12*, 3078. [CrossRef] [PubMed]
15. Zhang, P.; Han, Q.; Wu, J.; Zhang, Y.; Zhang, T. Mechanical properties of nano SiO_2 reinforced reactive powder concrete under different curing conditions. *Constr. Build. Mater.* **2023**, *356*, 129123. [CrossRef]
16. Hamada, H.; Shi, J.; Yousif, S.T.; Al Jawahery, M.; Tayeh, B.; Jokhio, G. Use of nano-silica in cement-based materials—A comprehensive review. *J. Sustain. Cem.-Based Mater.* **2023**, *12*, 1286–1306. [CrossRef]
17. Hou, P.; Kawashima, S.; Kong, D.; Corr, D.J.; Qian, J.; Shah, S.P. Effects of colloidal nanosilica on rheological and mechanical properties of fly ash–cement mortar. *Cem. Concr. Compos.* **2013**, *35*, 12–22. [CrossRef]

Disclaimer/Publisher's Note: The statements, opinions and data contained in all publications are solely those of the individual author(s) and contributor(s) and not of MDPI and/or the editor(s). MDPI and/or the editor(s) disclaim responsibility for any injury to people or property resulting from any ideas, methods, instructions or products referred to in the content.